A New Finite-Differencing Scheme for the Tracer Transport Equation

GARY L. RUSSELL

Institute for Space Studies, Goddard Space Flight Center, NASA, New York, NY 10025

JEAN A. LERNER

Sigma Data Services Corporation, New York, NY 10025

ABSTRACT

A new finite-differencing scheme for solving the tracer transport equation given prescribed winds is presented. The prognostic quantities predicted by the new scheme are the mean concentration and its spatial gradients. In one and two-dimensional tests using uniform air masses, the new scheme is roughly comparable to a fourth-order differencing scheme in accuracy. When the air masses are not uniform, the new scheme is superior to fourth-order differencing. An application of the schemes to three-dimensional tracer modeling is included.

1. Introduction

This paper introduces a new finite-differencing scheme, called the "slopes scheme", to solve the tracer transport equation. The slopes scheme is basically an upstream scheme but it uses and predicts the spatial gradients of concentration in addition to the mean concentration within each grid box.

Several authors (Crowley, 1968; Kreis and Oliger, 1972; Anderson and Fattahi, 1974; Purnell, 1976; Mahlman and Sinclair, 1977) have reviewed numerical schemes to solve the transport equation. Here we examine three well known schemes—the upstream, second- and fourth-order schemes—and compare them to the slopes scheme. All four schemes were tested using periodic models in one and two dimensions. They were also applied to a global three-dimensional model with winds generated by our general circulation model. We will outline some properties of the schemes in this introduction, with a more quantitative discussion to follow.

In all our tests the upstream scheme showed itself to be highly diffusive, but it displays a negligible phase lag and is only moderately affected by air mass variations. In one and two-dimensional tests with uniform air masses, the second-order scheme generates a phase lag and has other inaccuracies, while the fourth-order scheme advects the initial distribution very well. But when the air masses are not uniform, both these higher-order schemes produce "noisy" patterns that depend on the magnitude of the air mass perturbations. When used in our three-dimensional tracer models, where there are large variations in air mass, these schemes are unable to maintain anything like a coherent tracer distribution.

In contrast, the slopes scheme produces smooth distributions, has no phase lag, is only marginally affected by air mass variations, and shows little diffusion.

There are various modifications which are commonly applied to the second- and fourth-order schemes to prevent negative concentrations, generally at the expense of greater diffusion. In applications where it is necessary to have both positive and negative tracer concentrations or when small variations exist on a large mean value (e.g., carbon dioxide), such modifications are inapplicable. Hence, in this paper we mainly discuss the schemes in their pure form.

2. The finite-difference equations for the schemes

R, the concentration of a tracer with respect to air, in the absence of sources or sinks is governed by the differential equation

$$\frac{\partial R}{\partial t} + \mathbf{V} \cdot \nabla R = 0, \tag{1}$$

where $\mathbf{V}$ is a specified velocity, t is time, and ∇ is the spatial gradient operator. Assuming that mass of air is conserved, the density of air ρ satisfies the continuity equation

$$\frac{\partial \rho}{\partial t} + \nabla \cdot \rho \mathbf{V} = 0. \tag{2}$$

The conservative or flux form of the tracer transport equation is determined from (1) and (2):

$$\frac{\partial \rho R}{\partial t} + \nabla \cdot \rho \mathbf{V} R = 0. \tag{3}$$
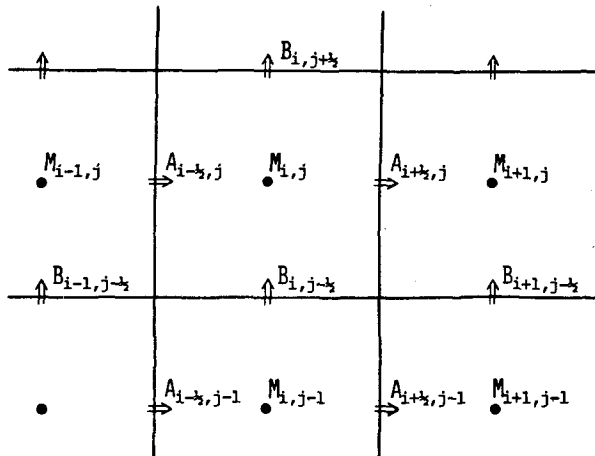
FIG. 1. Delineation of grid boxes and location of air mass and air mass fluxes in the two-dimensional model.

The numerical schemes discussed in this paper approximate (3) with finite-difference equations. The equations are written in two dimensions in Cartesian coordinates (x, y) so that the reader can see how they can be generalized to three dimensions or reduced to one dimension.

We adopt the convention that subscripts (i, j) refer to discrete locations in the x, y directions with grid spacings $\Delta x, \Delta y$, and superscripts (n) refer to discrete times with time interval Δt. We assume that Δx, Δy and Δt are uniform in time and space. The mass of air in a grid box is $M \approx \rho \Delta x \Delta y$ and the air mass fluxes are $A \approx \rho u \Delta t \Delta y$, $B \approx \rho v \Delta t \Delta x$, where u, v are the components of V in the x and y directions, re-

spectively. The spatial staggering of these quantities is shown in Fig. 1. The mass fluxes $A^{n+1/2}$ and $B^{n+1/2}$ are temporally staggered because they represent the mass of air crossing the edge of a grid box during the time $n\Delta t$ to $(n + 1)\Delta t$.

We assume that M, A and B are known functions of time and space and that (2) has been solved by the finite-difference equation

$$M^{n+1} - M^n + A_{i+1/2}^{n+1/2} - A_{i-1/2}^{n+1/2}$$
$$+ B_{j+1/2}^{n+1/2} - B_{j-1/2}^{n+1/2} = 0. \quad (4)$$

Here and in the remainder of the paper we will explicitly write only those indices which are necessary for clarity.

Figs. 2, 3 and 4 illustrate the upstream, second-order and slopes schemes in one dimension using forward explicit time steps (FS). (The fourth-order scheme is not easily represented this way.) The second- and fourth-order schemes are unstable with forward time steps, so in practice we use the leapfrog (LF) method for them. To simplify the notation for the leapfrog time steps we set

$$A_{i+1/2}^n = A_{i+1/2}^{n-1/2} + A_{i+1/2}^{n+1/2}, \quad (5)$$

and similarly for B.

The upstream scheme is

$$(MR)^{n+1} - (MR)^n + F_{i+1/2} - F_{i-1/2}$$
$$+ G_{j+1/2} - G_{j-1/2} = 0, \quad (6)$$

where

$$F_{i+1/2} = \begin{cases} A_{i+1/2}^{n+1/2} R_i & \text{when } A_{i+1/2}^{n+1/2} \geqslant 0, \\ A_{i+1/2}^{n+1/2} R_{i+1} & \text{when } A_{i+1/2}^{n+1/2} < 0. \end{cases} \quad (7)$$
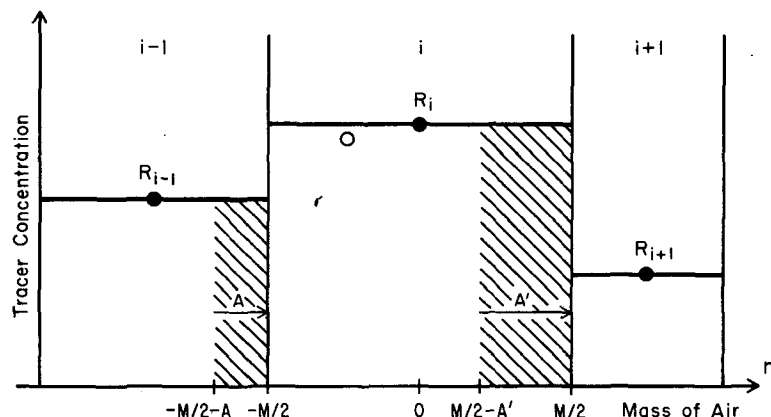

FIG. 2. Diagram of the upstream scheme in one dimension. The abscissa is air mass, ordinate is tracer concentration. The mean concentrations at the beginning of a time step for three grid boxes are R_{i-1}, R_i, and R_{i+1} (solid circles). M $(=M_i)$ is the mass of air in grid box i; A $(=A_{i-1/2})$ is air mass flux from box $i - 1$ into i; A' $(=A_{i+1/2})$ is air mass flux from i into $i + 1$. (In this example both A and A' are positive. An alternative view is that the mass and tracer are fixed, while the grid edges are moved to the left during the time step.) The hatched areas AR_{i-1} and $A'R_i$ are the masses of tracer moving into and out of grid box i, respectively. The mean tracer concentration in grid box i at the end of the time steps is $(MR_i + AR_{i-1} - A'R_i)/(M + A - A')$ (open circle).
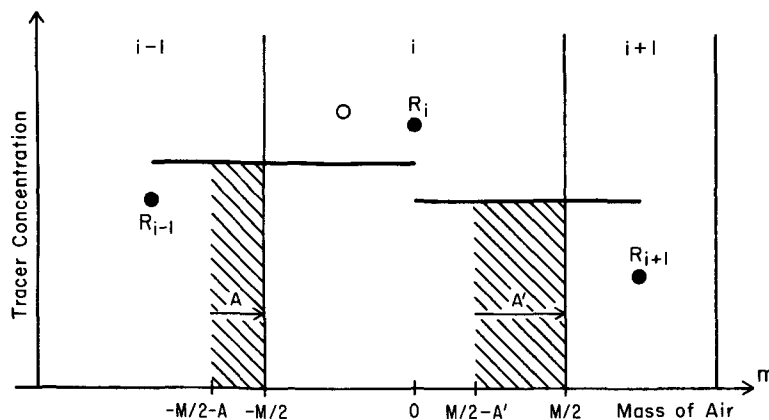
FIG. 3. Diagram of the second-order scheme in one dimension. For nomenclature, refer to Fig. 2. The hatched areas $A(R_{i-1} + R_i)/2$ and $A'(R_i + R_{i+1})/2$ are the masses of tracer moving into and out of grid box i. The mean concentration in grid box i at the end of the time step is $[MR_i + A(R_{i-1} + R_i)/2 - A'(R_i + R_{i+1})/2]/(M + A - A')$ (open circle).

The definition of G is symmetric: A is replaced by B and i is replaced by j.

The second-order scheme is

$$(MR)^{n+1} - (MR)^{n-1} + \tfrac{1}{2}A_{i+1/2}(R_i + R_{i+1})$$
$$- \tfrac{1}{2}A_{i-1/2}(R_{i-1} + R_i) + \tfrac{1}{2}B_{j+1/2}(R_j + R_{j+1})$$
$$- \tfrac{1}{2}B_{j-1/2}(R_{j-1} + R_j) = 0. \quad (8)$$

The fourth-order scheme is

$$(MR)^{n+1} - (MR)^{n-1}$$
$$+ \tfrac{1}{12}A_{i+1/2}(-R_{i-1} + 7R_i + 7R_{i+1} - R_{i+2})$$
$$- \tfrac{1}{12}A_{i-1/2}(-R_{i-2} + 7R_{i-1} + 7R_i - R_{i+1})$$

$$+ \tfrac{1}{12}B_{j+1/2}(-R_{j-1} + 7R_j + 7R_{j+1} - R_{j+2})$$
$$- \tfrac{1}{12}B_{j-1/2}(-R_{j-2} + 7R_{j-1} + 7R_j - R_{j+1}) = 0. \quad (9)$$

A detailed derivation of the slopes scheme will be found in Section 3. Here we present the difference equations with a brief explanation. The slopes scheme uses several prognostic quantities to represent the tracer distribution within a grid box: the mean concentration R and the slope of concentration in each direction multiplied by the spatial interval in that direction. In two dimensions let the vector slope $\mathbf{S} = (S, T)$ so that $R + \tfrac{1}{2}S$ is the average concentration at the right edge of the grid box and $R + \tfrac{1}{2}T$ is the average concentration at the top edge. We note that the concentration is discontinuous at the edges. The
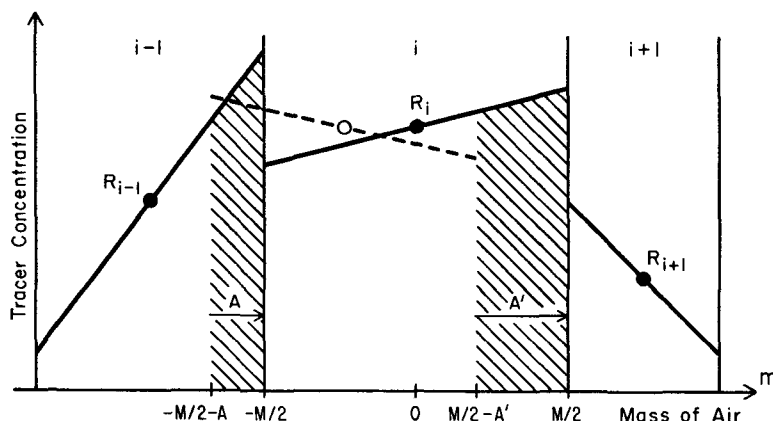

FIG. 4. Diagram of the slopes scheme in one dimension. For nomenclature refer to Fig. 2. The hatched areas are the masses of tracer moving into and out of grid box i. The heavy solid lines indicate the piecewise linear distribution of concentration $f(m)$ at the beginning of a time step. The dashed line segment is the least-squares fit line for the function $f(m)$ in the interval $(-M/2-A, M/2-A')$. It determines the linear distribution in grid box i at the end of the time step; its center point coincides with the mean concentration (open circle).

scheme can be written

$$(MR)^{n+1} - (MR)^n + F_{i+1/2} - F_{i-1/2} + G_{j+1/2} - G_{j-1/2} = 0, \tag{10}$$

$$(MS)^{n+1} - (MS)^n + \{M_i[6(F_{i-1/2} + F_{i+1/2}) - (A_{i+1/2} - A_{i-1/2})S_i] - 6(A_{i-1/2} + A_{i+1/2})$$

$$\times (M_iR_i - F_{i+1/2} + F_{i-1/2}) + P_{i+1/2} - P_{i-1/2}\}/(M_i - A_{i+1/2} + A_{i-1/2}) + E_{j+1/2} - E_{j-1/2} = 0, \tag{11}$$

$$(MT)^{n+1} - (MT)^n + \{M_j[6(G_{j-1/2} + G_{j+1/2}) - (B_{j+1/2} - B_{j-1/2})T_j] - 6(B_{j-1/2} + B_{j+1/2})$$

$$\times M_jR_j - G_{j+1/2} + G_{j-1/2}) + Q_{j+1/2} - Q_{j-1/2}\}/(M_j - B_{j+1/2} + B_{j-1/2}) + D_{i+1/2} - D_{i-1/2} = 0, \tag{12}$$

where

$$F_{i+1/2} = \begin{cases} A_{i+1/2}[R_i + \tfrac{1}{2}(1 - A_{i+1/2}/M_i)S_i] & \text{when} \quad A_{i+1/2} \geq 0 \\ A_{i+1/2}[R_{i+1} - \tfrac{1}{2}(1 + A_{i+1/2}/M_{i+1})S_{i+1}] & \text{when} \quad A_{i+1/2} < 0, \end{cases} \tag{13}$$

$$P_{i+1/2} = \begin{cases} A_{i+1/2}[(A_{i+1/2})^2 S_i/M_i - 6F_{i+1/2}] & \text{when} \quad A_{i+1/2} \geq 0 \\ A_{i+1/2}[(A_{i+1/2})^2 S_{i+1}/M_{i+1} - 6F_{i+1/2}] & \text{when} \quad A_{i+1/2} < 0, \end{cases} \tag{14}$$

$$D_{i+1/2} = \begin{cases} A_{i+1/2}T_i & \text{when} \quad A_{i+1/2} \geq 0 \\ A_{i+1/2}T_{i+1} & \text{when} \quad A_{i+1/2} < 0. \end{cases} \tag{15}$$

G, Q and E are defined the same as F, P and D, respectively, by replacing A with B, S with T, and i with j.

Note that (10) is formally identical to the upstream scheme (6) but that the definitions of F and G have additional terms. Also, note that in one dimension (12) disappears, as do D, G, Q and E. In three dimensions we require additional terms for (10), (11) and (12), as well as an equation for the slope in the third direction.

3. Derivation of the slopes scheme

We begin our derivation in one dimension, so that B, the mass flux in the y direction, is zero. At the beginning of time step n we establish a linear coordinate m in the x direction whose unit is mass of air and whose zero point is the center of the grid box i. (m is a Lagrangian coordinate and is more rigorously defined at the beginning of Section 4. Also, see Fig. 4.) We determine a piecewise linear function which represents the distribution of tracer concentration as a function of mass:

$$f(m) = \begin{cases} \vdots \\ R_{i-1} + (m + \tfrac{1}{2}M_{i-1} + \tfrac{1}{2}M_i)S_{i-1}/M_{i-1} & \text{when} \quad -M_{i-1} - \tfrac{1}{2}M_i < m < -\tfrac{1}{2}M_i \\ R_i + mS_i/M_i & \text{when} \quad -\tfrac{1}{2}M_i < m < \tfrac{1}{2}M_i \\ R_{i+1} + (m - \tfrac{1}{2}M_i - \tfrac{1}{2}M_{i+1})S_{i+1}/M_{i+1} & \text{when} \quad \tfrac{1}{2}M_i < m < \tfrac{1}{2}M_i + M_{i+1}. \\ \vdots \end{cases} \tag{16}$$

R_i is the average value of $f(m)$ in grid box i and S_i is $M_i \cdot \partial f/\partial m$ in grid box i. During the time step, $A_{i-1/2}$ is the air mass entering grid box i from the left and $A_{i+1/2}$ is leaving to the right. The slopes scheme fits $f(m)$ from $-\tfrac{1}{2}M_i - A_{i-1/2}$ to $\tfrac{1}{2}M_i - A_{i+1/2}$ by a new least-squares line segment, thus determining the mean concentration and slope for grid box i at the end of the time step.

Set

$$I = \int_{-1/2M_i - A_{i-1/2}}^{1/2M_i - A_{i+1/2}} [f(m) - ma - b]^2 dm \tag{17}$$

and calculate a and b from the two equations:

$$dI/da = 0, \tag{18}$$

$$dI/db = 0. \tag{19}$$

The new center of mass of grid box i with respect to the old coordinate is

$$c = \tfrac{1}{2}(-A_{i-1/2} - A_{i+1/2}). \tag{20}$$

The new values of R and S at time $n + 1$ are

$$R_i^{n+1} = ac + b, \tag{21}$$

$$S_i^{n+1} = a(M_i^n - A_{i+1/2} + A_{i-1/2}) = aM_i^{n+1}. \tag{22}$$

In addition, the least-squares-method guarantees tracer mass conservation:

$$\int_{-1/2M_i - A_{i-1/2}}^{1/2M_i - A_{i+1/2}} f(m)dm = (MR)_i^{n+1}. \tag{23}$$

To simplify the computer code we assume that the

air mass flux leaving a grid box does not exceed the mass of air in the box, i.e.,

$$A_{i+1/2} \leqslant M_i \qquad (24)$$

and

$$-A_{i-1/2} \leqslant M_i. \qquad (25)$$

These assumptions force the limits of integration in (17) and (23) to lie within the three boxes $i - 1$, i and $i + 1$. When they are not satisfied, the scheme becomes inaccurate. The same applies to our upstream scheme.

Using (16)–(23) together with the one dimensional analog of (4), Eqs. (10) and (11) can be derived for the one-dimensional case. For two dimensions (12) can readily be derived from (11) through symmetry. However, the extra terms E and D in (11) and (12) do not come directly from this derivation. In the case of (11), the E terms represent the upstream advection of S in the y direction.

For the slopes scheme to be accurate in two dimensions, one further adjustment is required. As already noted, the scheme basically advects into a grid box the air and tracer that was upstream of the box at an earlier time. As long as the vector wind is parallel to one coordinate axis, the scheme works very well (see Section 4 on one-dimensional tests.) However, when the vector wind is not parallel to an axis, each grid box should receive tracer from corner boxes as well as from side boxes. The contribution from the corner boxes is not taken into account in the scheme, and if the mass fluxes are large, this error can be significant enough to actually overwhelm the scheme.

One solution is to use small mass fluxes, which is equivalent to using small time steps. This works because the contribution from the corner boxes is proportional to Δt^2, whereas the contribution from the side boxes is proportional to Δt. The drawback to this solution is that it significantly increases the computer time required.

Another solution is to use spatial leapfrog (SLF) (see Fig. 5). We start using one-half the mass flux in the x direction and no flux in the y direction. Thereafter, on alternate steps we use the mass flux in the y direction or an average mass flux in the x direction. The flux in the other direction is zero. At the end of the integration, the last half mass flux in the x direction is used. It also can be understood as integrating (10), (11) and (12) but zeroing out A (and, consequently, also F, P and D) on odd time steps and zeroing out B (and, consequently, also G, Q and E) on even time steps.

Spatial leapfrog in two dimensions can dramatically improve the results of the slopes scheme (see Figs. 9 and 10.) It also can be used in the upstream scheme. SLF is not directly applicable to the second- and fourth-order schemes since it would interfere with their temporal leapfrog.
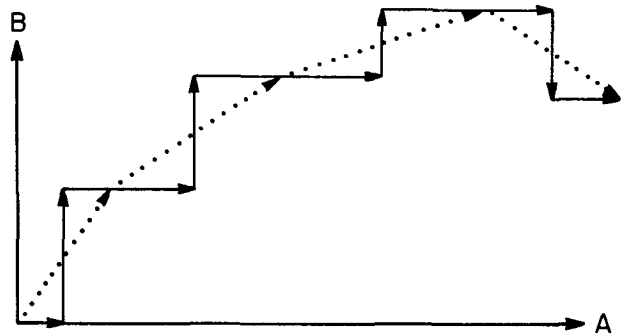

FIG. 5. Diagram of the spatial leapfrog method. The coordinates are the mass fluxes in two directions. The two-dimensional mass flux field (dotted arrows) for several time steps is separated into one-dimensional mass fluxes (solid arrows) for different overlapping time steps.

4. Numerical experiments in one dimension

Using the notation of Section 2, we replace V by u (since we are interested in one dimension) and set $a = \rho u$. (2) is then written as

$$\frac{\partial \rho}{\partial t} + \frac{\partial a}{\partial x} = 0. \qquad (26)$$

Given arbitrary functions $\rho(x, t)$ and $a(x, t)$ satisfying (26), there exist functions $m(x, t)$ such that

$$\rho = \partial m/\partial x \qquad (27)$$

and

$$a = -\partial m/\partial t. \qquad (28)$$

m may be a global function if the spatial domain is simply connected, otherwise m will only be local. If ρ is positive, m is a monotonically increasing function of x and can be used as an alternative reference frame. We refer to m as the mass coordinate. Figs. 2, 3 and 4 use m as the abscissa. The implications of the two reference frames with which to view R will be discussed in Section 7.

The solution of the one dimensional analog of (3) is that $R(x, t)$ can be factored through the function $m(x, t)$ and another function $\tilde{R}(m)$, i.e., $R(x, t) = \tilde{R}[m(x, t)]$. The initial condition $R(x, 0)$ determines $\tilde{R}(m)$ which in turn determines $R(x, t)$ for $t > 0$. [In Section 3 and in Fig. 4, $f(m)$ is a piecewise linear function that approximates $\tilde{R}(m)$.]

Our one-dimensional model requires that the spatial coordinate be periodic (i.e., a circle) with period 1. In this case, m can only be locally defined. $\rho(x + k, t) = \rho(x, t)$ and similarly for a and R, where k is an integer. To simplify the model, we assume that ρ is constant in time and, by virtue of (26), that $a = \rho u$ is constant in space. N revolutions are completed at time τ when:

$$N \int_0^1 \rho(x)dx = \int_0^\tau a(t)dt. \qquad (29)$$

TABLE 1. rms error dependence on grid resolution for the one dimensional model.

IM	Upstream	2nd order	4th order	Slopes
8	261.26	262.72	337.87	150.09
16	244.00	329.39	208.39	72.10
32	223.67	223.37	61.99	22.11
64	189.81	98.50	13.31	5.83
128	146.91	32.07	3.29	1.58
256	102.11	10.31	0.83	0.43
512	63.94	3.27	0.21	0.12

The analysis in the preceeding paragraph and the fact that $m(x, \tau) = m(x - N, 0)$ shows that for an exact analytic solution, the distribution of R after N revolutions is identical in space to its initial distribution.

Set

$$R(x, 0) = \begin{cases} 0 & \text{when} \quad -\frac{1}{2} \leqslant x \leqslant -\frac{1}{8} \\ 1000(1 - 2(8x)^2 + (8x)^4) \\ & \text{when} \quad -\frac{1}{8} \leqslant x \leqslant \frac{1}{8} \\ 0 & \text{when} \quad \frac{1}{8} \leqslant x \leqslant \frac{1}{2} . \end{cases} \quad (30)$$

For our numerical model

$$R_i^0 = \frac{1}{\Delta x} \int_{\Delta x(i-1/2)}^{\Delta x(i+1/2)} R(x, 0)dx, \quad (31)$$

where Δx is the length of each grid box. For the slopes scheme we initially determine S_i as the slope of the least-squares-fit line segment of the function $R(x, 0)$ from $\Delta x(i - \frac{1}{2})$ to $\Delta x(i + \frac{1}{2})$ multiplied by Δx. (Setting the initial slopes S_i to zero introduces a small error which decreases as the number of revolutions increases.)

There are five important variable parameters in our model. These parameters determine intermediate parameters from which the fields M and A are derived. The five important parameters are: 1) *IM*: the number of grid boxes around the circle; 2) α: a dimensionless parameter which measures the ratio of the air mass flux to air mass, assuming uniform density; 3) *NREV*: the number of revolutions after which time comparisons will be made; 4) *AMPM*: the magnitude of the random perturbations of the air mass field, a discrete function of space; and 5) *AMPA*: the magnitude of the random perturbations of the air mass flux field, a discrete function of time. When *AMPM* and *AMPA* are zero, M and A are uniform, i.e., constant in time and space. When *AMPM* or *AMPA* is not zero, M or A has random perturbations.

The definitions of the intermediate parameters used in the model are:

$\Delta x = 1/IM$ the equal length of each grid box

$\rho_{\text{uniform}} = 1$ the uniform density of air

$u_{\text{uniform}} = 1$ the uniform wind speed

$\Delta t = \alpha \cdot \Delta x / u_{\text{uniform}}$ the time step

M_{uniform} the uniform mass of air in a grid box
$= \Delta x \cdot \rho_{\text{uniform}}$

A_{uniform} the uniform mass of air crossing from one grid box to an adjacent box during a time step
$= \Delta t \cdot \rho_{\text{uniform}} \cdot u_{\text{uniform}}$

r a random variable with equi-probability in the interval $(-1, 1)$, it may be a discrete function of space or a discrete function of time.

The fields M and A used by the schemes are: $M = M_{\text{uniform}}(1 + AMPM \cdot r)$, the mass of air, a discrete function of space; $A = A_{\text{uniform}}(1 + AMPA \cdot r)$, the air mass flux, a discrete function of time. Since we assume that ρ is constant in time, M must be constant in time and A must be constant in space. The prognostic quantities R and S determined by the schemes have already been defined.

The primary time step for all the schemes is Δt. This means that for the second- and fourth-order schemes, which use leap frog, the odd solution is known when $t = (n + \frac{1}{2}) \cdot \Delta t$ and the even solution is known when $t = n \cdot \Delta t$, where n is an integer. To start the leapfrog, the first odd solution at $t = \frac{1}{2}\Delta t$ is determined by using a half forward step. (Improving the start up procedure by using smaller steps had a negligible effect on the results.)

The five variable parameters of the model were changed separately to determine the sensitivity of the schemes to each of them. The default values for these tests were

$$IM = 64,$$
$$\alpha = 0.125,$$
$$NREV = 1,$$
$$AMPM = 0,$$
$$AMPA = 0.$$

The tracer distribution at the end of the integration time was subtracted from the initial distribution to obtain the root-mean-square (rms) error over the domain. A perfect scheme would have zero error. The results of the tests are shown in Tables 1–5.

TABLE 2. rms error dependence on α for the one-dimensional model.

α	Upstream	2nd order	4th order	Slopes
0.0156	196.54	98.77	13.64	6.78
0.0313	195.64	98.76	13.63	6.64
0.0625	193.78	98.70	13.56	6.36
0.125	189.81	98.50	13.31	5.83
0.25	180.67	97.66	12.36	4.89
0.5	155.21	94.27	9.75	3.43
1.0	0.0	80.12	25.46	0.0

The tables show that in most cases the rms error of the slopes scheme is usually at least half that of the fourth-order scheme, which, in turn, has an rms error considerably less than that of the second-order and upstream schemes. Although one might expect that doubling the grid resolution should reduce the error by a factor of 2^2 in the second-order scheme or 2^4 in the fourth-order scheme, that was not the case in our experiments. Table 1 shows that for a fine mesh, doubling the resolution reduces the error by a factor of 3 for the second-order scheme and by a factor of 4 for the fourth-order and slopes schemes. Table 2 shows that each scheme works best for its longest time step before reaching numerical instability. For $\alpha = 1$, the schemes are at the edge of stability.

Table 4 shows that the fourth-order scheme is very sensitive to random deviations in the air mass fields. The second-order scheme is even more sensitive, but because of its larger rms error, the degradation is not reflected in the table. When $AMPM = 1$, the uniform air mass flux exceeds the air mass for 6% of the grid boxes, causing the schemes to be unstable.

Table 5 shows that all the schemes are fairly independent of variations in the air mass fluxes. When $AMPA = 8$, the air mass flux exceeds the uniform air mass for 6% of the grid boxes, again causing the schemes to be somewhat unstable.

The schemes are compared with each other and with the analytic solution in Figs. 6, 7 and 8. The final distributions of the schemes using the default values, except that NREV = 8, are shown in Fig. 6. The second-order scheme shows a large phase lag and a significant decrease in the maximum value of the peak, as well as large negative values. The maximum value of the fourth-order scheme is nearly that of the initial distribution; however, there is some phase lag and several small extraneous ripples. The peak of the slopes scheme is somewhat lower, but it is more symmetric and has only a few small ripples.

Fig. 7, with $AMPM = 0.25$ shows the enormous sensitivity of the second-order scheme to variations in the air mass field. Within the region of the initial peak, the fourth-order scheme is relatively unaffected; however, it is quite ragged elsewhere. In con-

trast, both the upstream and slopes schemes show almost no effects.

Fig. 8 shows more clearly the degradation of the fourth-order scheme when there are variations in the mass field and when NREV is increased. We used NREV = 64 and $AMPM = 0.25$ for the fourth-order and slopes scheme, and in addition we included the fourth-order scheme with $AMPM = 0$. (The slopes scheme with uniform mass is similar to the one in the figure but has a higher peak.)

5. Numerical experiments in two dimensions

We extend the analysis performed at the beginning of Section 4 to two dimensions. V becomes (u, v) and we set $a = \rho u$, $b = \rho v$. We put a, b and ρ into a vector $\mathbf{P} = (a, b, \rho)$. (2) is rewritten as

$$\nabla \cdot \mathbf{P} = 0, \tag{32}$$

where the ∇ operator is now $(\partial/\partial x, \partial/\partial y, \partial/\partial t)$. Given an arbitrary function $\mathbf{P}(x, y, t)$ satisfying (32), there exist functions $m(x, y, t)$ and $n(x, y, t)$ such that

$$\mathbf{P} = \nabla m \times \nabla n. \tag{33}$$

m and n may be global functions if the spatial domain is a simply connected planar domain. When the Jacobian operator $J(m, n/x, y) = \rho$ is positive, (m, n) is one to one on (x, y), i.e., (m, n) can be used as an alternative reference frame called the two-dimensional mass coordinates.

The two-dimensional analog of (1) is

$$\nabla m \times \nabla n \cdot \nabla R = 0. \tag{34}$$

TABLE 4. rms error dependence on the amplitude of the random perturbations of the mass field for the one-dimensional model.

AMPM	Upstream	2nd order	4th order	Slopes
0.0	189.81	98.50	13.31	5.83
0.0313	189.97	99.33	15.01	5.66
0.0625	190.19	100.49	19.57	5.56
0.125	190.76	103.72	31.96	5.60
0.25	192.45	112.77	59.77	6.60
0.5	197.84	140.76	116.41	11.25
1.0	214.02	247.45	225.45	26.24

TABLE 3. rms error dependence on the number of revolutions for the one-dimensional model.

NREV	Upstream	2nd order	4th order	Slopes
1	189.81	98.50	13.31	5.83
2	225.76	163.99	20.48	9.37
4	253.83	228.70	25.58	15.00
8	276.30	280.14	39.54	24.10
16	287.33	330.21	67.75	38.79
32	288.80	413.26	100.96	59.93
64	288.82	334.55	146.26	85.96

TABLE 5. rms error dependence on the amplitude of the random perturbations of the mass flux field for the one-dimensional model.

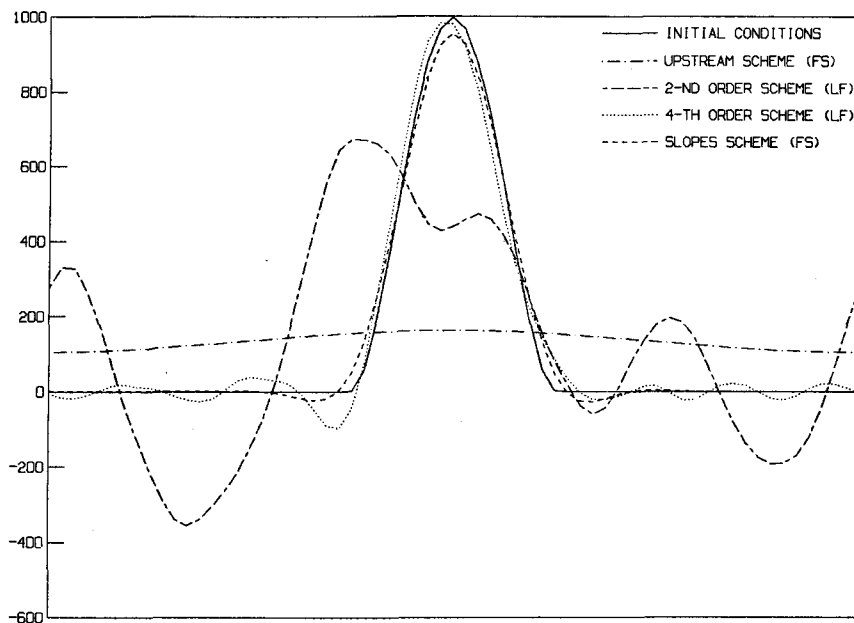| AMPA	Upstream	2nd order	4th order	Slopes
0.0	189.81	98.50	13.31	5.83
0.25	189.63	98.47	13.28	5.81
0.5	189.08	98.42	13.18	5.75
1.0	186.83	98.24	13.08	5.51
2.0	193.15	97.72	12.00	5.46
4.0	209.90	91.76	10.50	6.67
8.0	207.58	73.51	37.61	6.84

FIG. 6. One-dimensional model with uniform mass field. The parameters used are $IM = 64$, $\alpha = 0.125$, $NREV = 8$, $AMPM = AMPA = 0$. The abscissa is the model's spatial coordinate, the ordinate is tracer concentration.

Again, R can be factored through (m, n) and another function $\tilde{R}(m, n)$ as $R(x, y, t) = \tilde{R}[m(x, y, t), n(x, y, t)]$. R is completely determined by the initial condition $R(x, y, 0)$ and the functions m and n which solve (32).

This analysis and the existence of mass coordinates can be extended to higher dimensions. Their implications will be discussed in Section 7.

Our two-dimensional model is symmetric in the two directions and is doubly periodic (hence topologically a torus) with periods 1. We assume that ρ is constant in time and that $a = \rho u = \rho v$ is constant in space. As in the one-dimensional case, after N revolutions at time τ, $R(x, y, \tau) = R(x - N, y - N, 0) = R(x, y, 0)$.
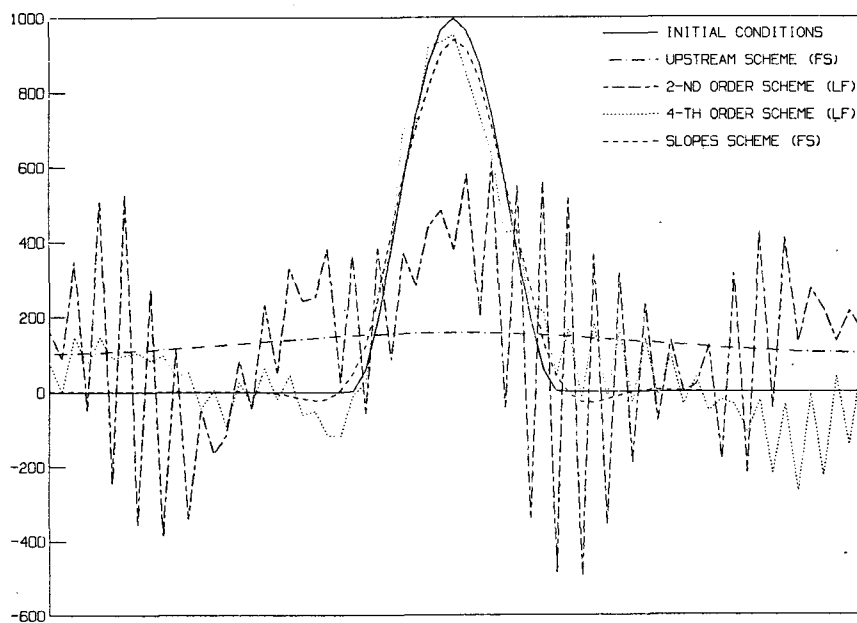
The initial distribution is
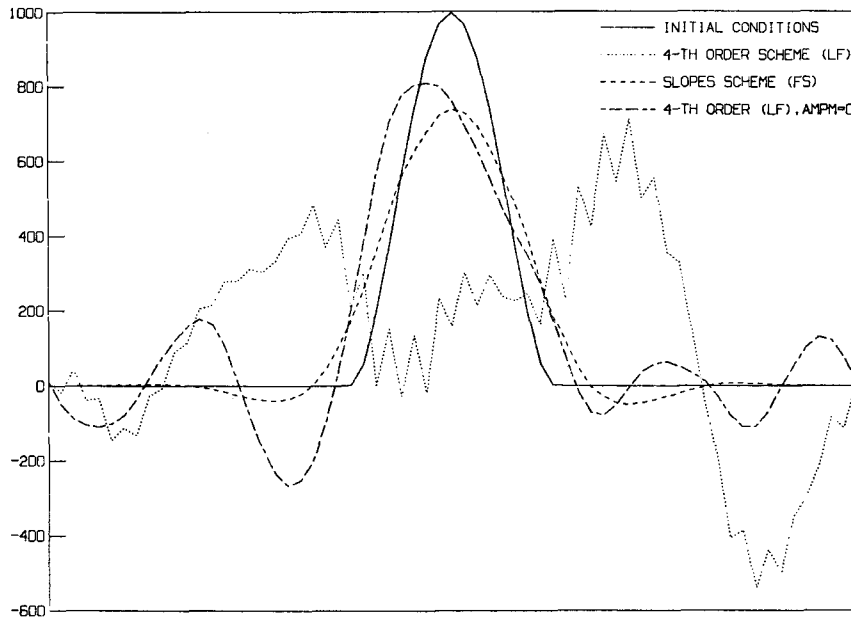

FIG. 7. As in Fig. 6 except $AMPM = 0.25$.

FIG. 8. Fourth-order and slopes schemes after 64 revolutions. The common parameters are $IM = 64$, $\alpha = 0.125$, $NREV = 64$, $AMPA = 0$. Both schemes are shown with $AMPM = 0.25$; the fourth order scheme with $AMPM = 0$ is included.

$R(x, y, 0)$

$$= \begin{cases} 0 & \text{when} \quad -\tfrac{1}{2} \leqslant x \leqslant -\tfrac{1}{8} \quad \text{or} \quad -\tfrac{1}{2} \leqslant y \leqslant -\tfrac{1}{8} \\ 1000[1 - 2(8x)^2 + (8x)^4][1 - 2(8y)^2 + (8y)^4] \\ \quad \text{when} \quad -\tfrac{1}{8} \leqslant x, y \leqslant \tfrac{1}{8} \\ 0 & \text{when} \quad \tfrac{1}{8} \leqslant x \leqslant \tfrac{1}{2} \quad \text{or} \quad \tfrac{1}{8} \leqslant y \leqslant \tfrac{1}{2}. \end{cases}$$

(35)

For the discrete model

$$R_{i,j}^0 = \frac{1}{\Delta x \cdot \Delta y} \int_{\Delta y(j-1/2)}^{\Delta y(j+1/2)} \int_{\Delta x(i-1/2)}^{\Delta x(i+1/2)} R(x, y, 0)dxdy,$$

(36)

where Δx and Δy are the lengths of each grid box.

For the slopes scheme, the initial $S_{i,j}$ is the slope of the least-squares-fit line in the x direction from $\Delta x(i - \tfrac{1}{2})$ to $\Delta x(i + \tfrac{1}{2})$ of the function $R(x, y, 0)$ integrated from $\Delta y(j - \tfrac{1}{2})$ to $\Delta y(j + \tfrac{1}{2})$ multiplied by $\Delta x/\Delta y$. The definition of the initial $T_{i,j}$ is symmetric.

The definitions of the parameters used in the two-dimensional model are carried over from the one-dimensional model. Since the model is symmetric, all spatial parameters are identical in the two directions and do not need to be defined separately. (In fact, all results are symmetric with the exception of the slopes scheme using spatial leapfrog.) Certain parameters need to be redefined from the one-dimensional case

$M_{\text{uniform}} = \Delta x \cdot \Delta y \cdot \rho_{\text{uniform}}$, the uniform mass of air in a grid box

$A_{\text{uniform}} = \Delta t \cdot \Delta x \cdot \rho_{\text{uniform}} \cdot u_{\text{uniform}}$, the uniform mass of air crossing the edge from one grid box to an adjacent box during a time step

$M_{i,j} = M_{\text{uniform}}(1 + (AMPM \cdot r_i)(1 + AMPM \cdot r_j)$, the mass of air, a discrete function of space.

The designation of the time steps and the initialization for the second- and fourth-order leapfrog are carried over from the one-dimensional model. The defaults for the variable parameters in the two-dimensional model are identical to those in the one-dimensional case. The sensitivity of the schemes to these parameters is shown in Tables 6–10. The slopes scheme with forward steps requires a smaller α (i.e., shorter time step) than $\tfrac{1}{8}$, but it is included at the default value for consistency.

The tables show that in most cases both the fourth-order and slopes (SLF) schemes have an rms error

TABLE 6. rms error dependence on grid resolution for the two-dimensional model.

IM	Upstream	2nd order	4th order	Slopes	Slopes (SLF)
8	89.34	101.96	120.94	66.43	67.71
16	89.25	122.18	85.84	56.46	42.99
32	87.79	93.42	27.29	67.00	17.66
64	79.36	43.69	5.94	42.33	4.29
128	65.38	14.40	1.48	20.46	0.92

TABLE 7. rms error dependence on α for the two-dimensional model.

α	Upstream	2nd order	4th order	Slopes	Slopes (SLF)
0.0156	81.44	43.89	6.14	6.24	4.85
0.0313	81.18	43.88	6.13	9.32	4.76
0.0625	80.62	43.84	6.09	17.52	4.60
0.125	79.36	43.69	5.94	42.33	4.29
0.25	76.00	43.05	5.52	∞	3.69
0.5	62.33	40.45	6.88	∞	2.59
1.0	∞	30.98	∞	∞	.02

TABLE 9. rms error dependence on the amplitude of the random perturbations of the mass field for the two-dimensional model.

AMPM	Upstream	2nd order	4th order	Slopes	Slopes (SLF)
0.0	79.36	43.69	5.94	42.33	4.29
0.0156	79.39	43.96	6.72	42.60	4.27
0.0313	79.44	44.40	8.72	42.85	4.26
0.0625	79.55	45.76	14.16	43.24	4.29
0.125	79.86	50.10	26.35	43.56	4.59
0.25	80.83	63.13	50.29	41.86	6.83
0.5	83.69	94.47	85.76	31.17	19.74

much lower than that of the upstream and second-order schemes (sometimes as much as an order of magnitude). Table 6 shows that the error reduction factor for doubling the resolution is similar for the one- and two-dimensional models, i.e., three for the second-order scheme and factors of 4 for the fourth-order and slopes (SLF) schemes.

Table 7 illustrates the statements made at the end of Section 3 regarding the slopes scheme, i.e., the scheme requires either small time steps or a spatial leapfrog mechanism. Table 9 is further evidence that the second- and fourth-order schemes are degraded by variations in the mass field. All of the schemes diverged for $AMPM = 1$.

Table 10 reiterates that the schemes are not strongly affected by variations in the air mass fluxes. The slopes (SLF) scheme was the only scheme to converge for $AMPA = 8$ in spite of the fact that 6% of the air mass fluxes exceed the uniform mass of the grid boxes.

Contour diagrams of the schemes are compared in Fig. 9 using the parameters $IM = 32$, $\alpha = 0.125$, $NREV = 2$, $AMPM = AMPA = 0$. They indicate the phase lags of the second- and fourth-order schemes and the artificial wave pattern those schemes generate. The slopes (SLF) scheme also has a wave pattern, but it is exeedingly damped. The regular slopes scheme indicates that it needs a smaller time step. The upstream scheme exhibits its well-known highly diffusive property.

Fig. 10 is to be compared to Fig. 9. All parameters are the same except that $AMPM = 0.25$. Note that the peak value has decreased for all the schemes. The slopes (SLF) scheme now has a small phase lag but is relatively unaffected otherwise. The second- and fourth-order schemes generate noisy unrealistic patterns.

6. Application to three-dimensional tracer modeling

The schemes were applied to a three-dimensional global tracer model which simulated the advection of ash that erupted from Mt. St. Helens in May 1980. The wind and air mass fields used in the experiments were generated by a general circulation model (Hansen et al., 1982) which is global in extent with 8° × 10° horizontal resolution and seven vertical layers numbered from the ground up. Dynamics is accomplished using Arakawa's scheme B. The model has annual and diurnal cycles and a realistic topography.

The idea of using the Mt. St. Helens eruption was partly whimsical, since we are not equipped to do a realistic simulation. However, it did provide an example of a simple application of the various schemes to the three-dimensional case.

The experiments represent the actual eruption in the following respects: 1) the tracer model uses a realistic global topography; 2) the emission in the model occurred at two adjoining grid boxes where

TABLE 8. rms error dependence on the number of revolutions for the two-dimensional model.

NREV	Upstream	2nd order	4th order	Slopes	Slopes (SLF)
1	79.36	43.69	5.94	42.33	4.29
2	89.01	71.19	9.12	171.18	7.34
4	94.83	95.96	11.27	∞	12.21
8	98.18	113.15	17.16	∞	19.42
16	99.46	127.03	29.26	∞	29.02
32	99.62	142.34	43.21	∞	40.23
64	99.62	127.32	61.79	∞	51.77

TABLE 10. rms error dependence on the amplitude of the random perturbations of the mass flux field for the two-dimensional model.

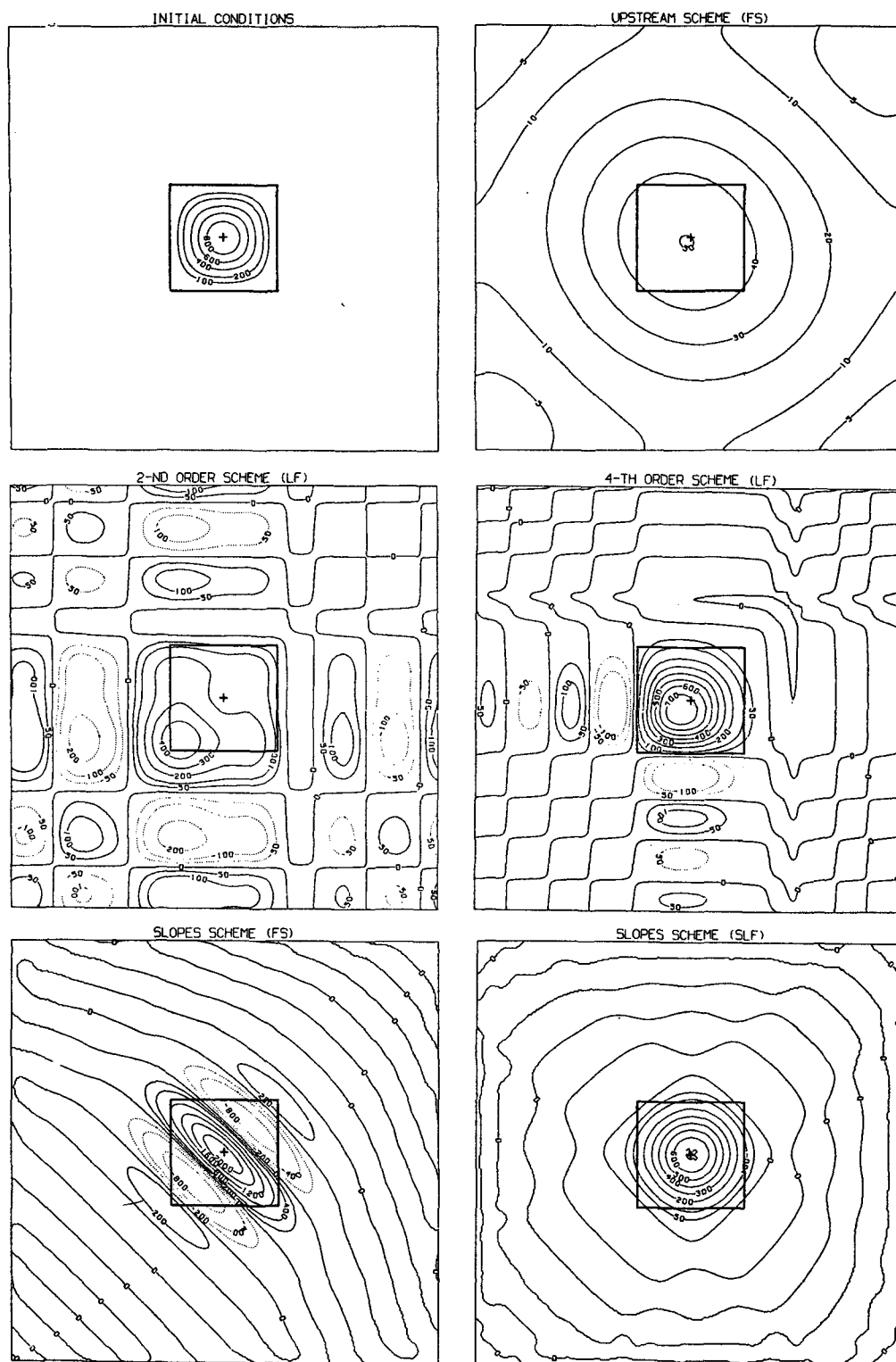| AMPA	Upstream	2nd order	4th order	Slopes	Slopes (SLF)
0.0	79.36	43.69	5.94	42.33	4.29
0.25	79.30	43.66	5.93	43.82	4.27
0.5	79.12	43.61	5.88	48.68	4.24
1.0	78.34	43.51	5.80	78.86	4.09
2.0	79.84	42.86	5.41	∞	4.26
4.0	82.42	39.23	8.10	∞	5.40
8.0	∞	∞	∞	∞	5.70

FIG. 9. The two-dimensional model with uniform air mass field. The parameters are $IM = 32$, $\alpha = 0.125$, $NREV = 2$, $AMPM = AMPA = 0$. Dotted contours have negative values. The square shows the nonzero extent of the initial distribution.
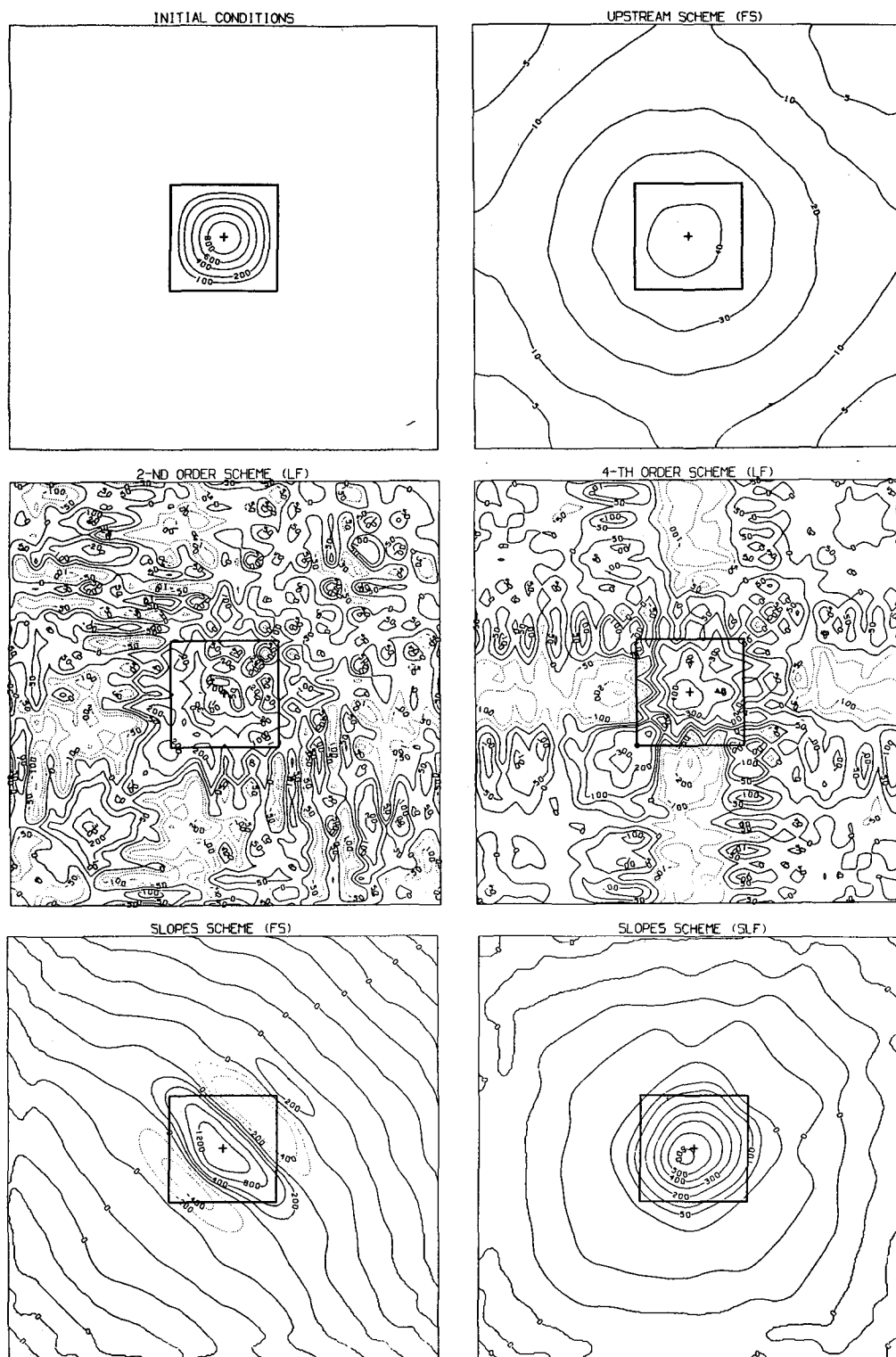
FIG. 10. As Fig. 9 except *AMPM* = 0.25.

Mt. St. Helens is centered; and 3) the winds in the model are comparable to May wind conditions in the real world. The unrealistic aspects of the experiments are: 1) actual wind observations were not used; 2) the model's emission occurred at layer 5 (236–400 mb) unlike the actual vertical distribution of ash; 3) the ash does not fall by gravity and is unaffected by rain; and 4) we did not allow vertical convection.

UPSTREAM SCHEME (FS)

SECOND ORDER SCHEME (LF)

FOURTH ORDER SCHEME (LF)

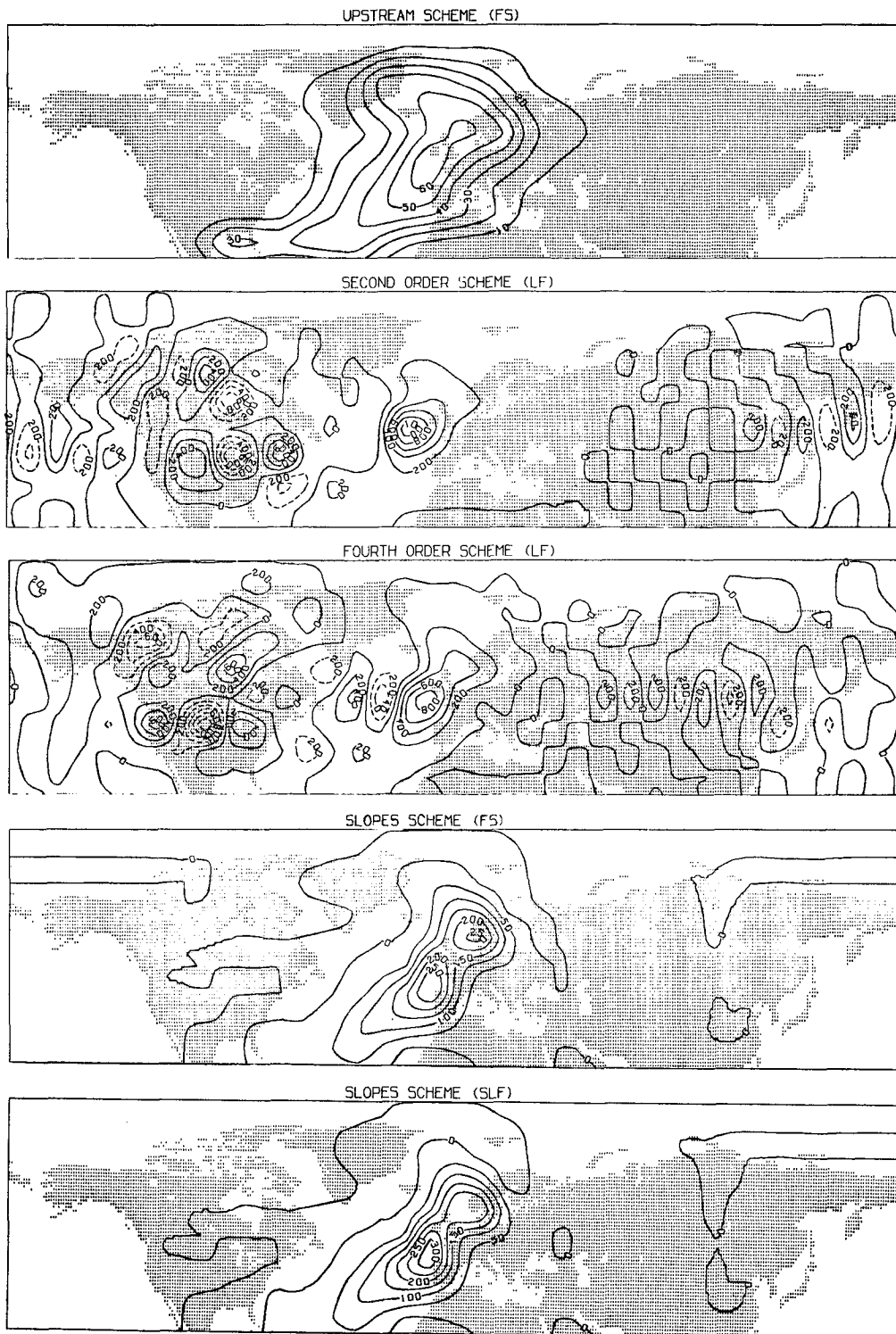SLOPES SCHEME (FS)

SLOPES SCHEME (SLF)

FIG. 11. Fifth layer concentrations for all the schemes after four days of integration.
Dashed contours have negative values.

The transport schemes were modified to use the GCM's regular latitude–longitude grid with fixed boundaries at the surface and at 10 mb. The longitudinal grid boxes at each pole are treated as single boxes. For the slopes schemes, the horizontal slopes at the polar grid boxes are set to zero. For the fourth-order scheme, the north–south advection near the poles uses the concentration of four grid boxes, one

SECOND ORDER SCHEME (LF) WITH LIMITS

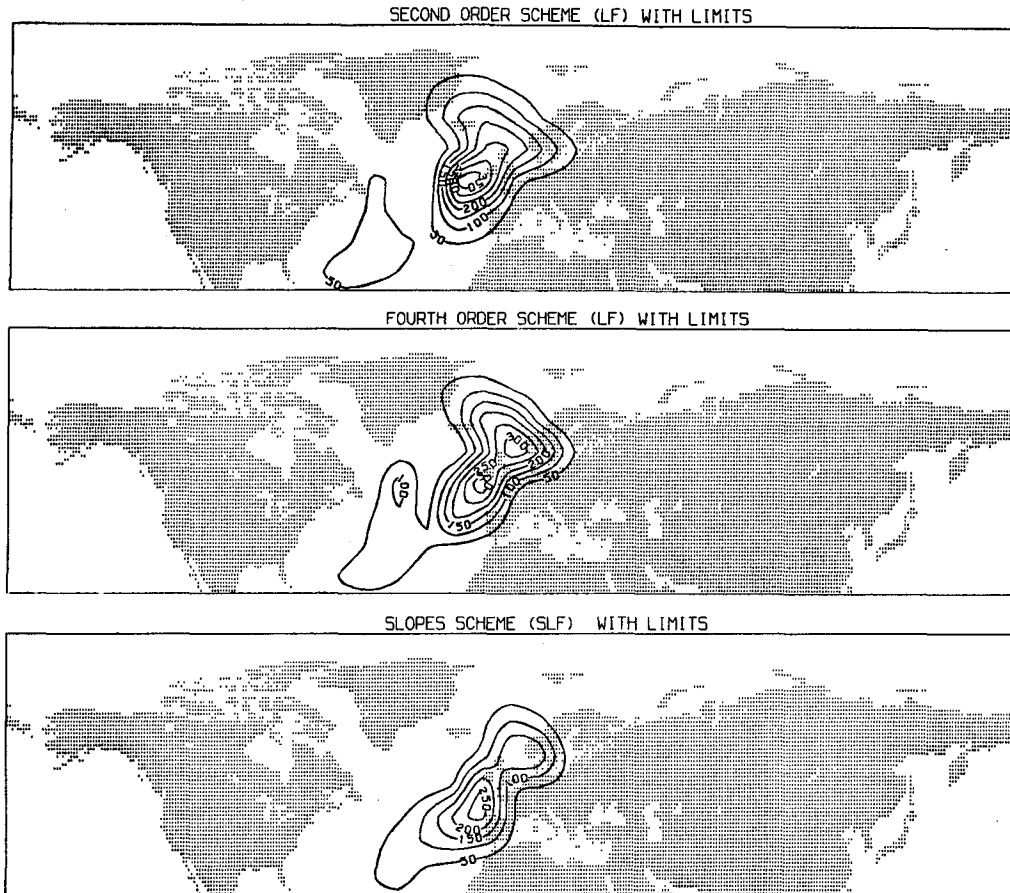FOURTH ORDER SCHEME (LF) WITH LIMITS

SLOPES SCHEME (SLF) WITH LIMITS

FIG. 12. Fifth-layer concentrations for the schemes with limits after four days of integration.

of which is on the other side of the pole; also, the vertical advection adjacent to the boundaries is a combination of second- and fourth-order differencing.

All the schemes except for the slopes (SLF) scheme use 1 h time steps. (This means that the two leapfrog solutions for the second- and fourth-order schemes are separated by 30 min.) Spatial leapfrog was applied to the slopes scheme every 6 h in the following ways:

- 1.5 h of east–west advection
- 3 h of north–south advection
- 1.5 h of east–west advection
- 6 h of vertical advection
- 1.5 h of east–west advection
- 3 h of north–south advection
- 1.5 h of east–west advection.

This method is dictated by the large east–west winds and the small east–west grid length. The vertical mass fluxes are generally small. The time steps for the schemes were arrived at empirically by testing each scheme with successively longer time steps until the results changed significantly.

Analysis of the prescribed wind fields revealed that in the upper atmosphere near the poles the air mass fluxes occasionally exceed the mass of a grid box for all the schemes. This occurs most often for the slopes (SLF) scheme because of its longer time step, but that scheme is better equipped than the other schemes to handle such instabilities (see Table 10).

Fig. 11 shows the fifth layer concentration predicted by the various schemes on 22 May, four days after the eruption. In general, the schemes behave in a way consistent with our one and two dimensional results: The upstream scheme is very diffuse, the second-order scheme shows some phase lag in the location of the peak concentration, and both the second- and fourth-order schemes show an unrealistic checkerboard pattern of positive and negative concentrations far from the ash cloud. This problem rapidly increases with time, rendering the schemes useless as a predictive tool after six days. One surprising result was that the slopes (FS) scheme shows none of the difficulties that motivated the use of spatial leapfrog in the two-dimensional case (see Section 5 and Figs. 9 and 10).

The slopes schemes also developed large areas of small negative concentration, especially in the first, third and seventh layers (not shown in the figures).

SECOND ORDER SCHEME (LF) WITH LIMITS

FOURTH ORDER SCHEME (LF) WITH LIMITS

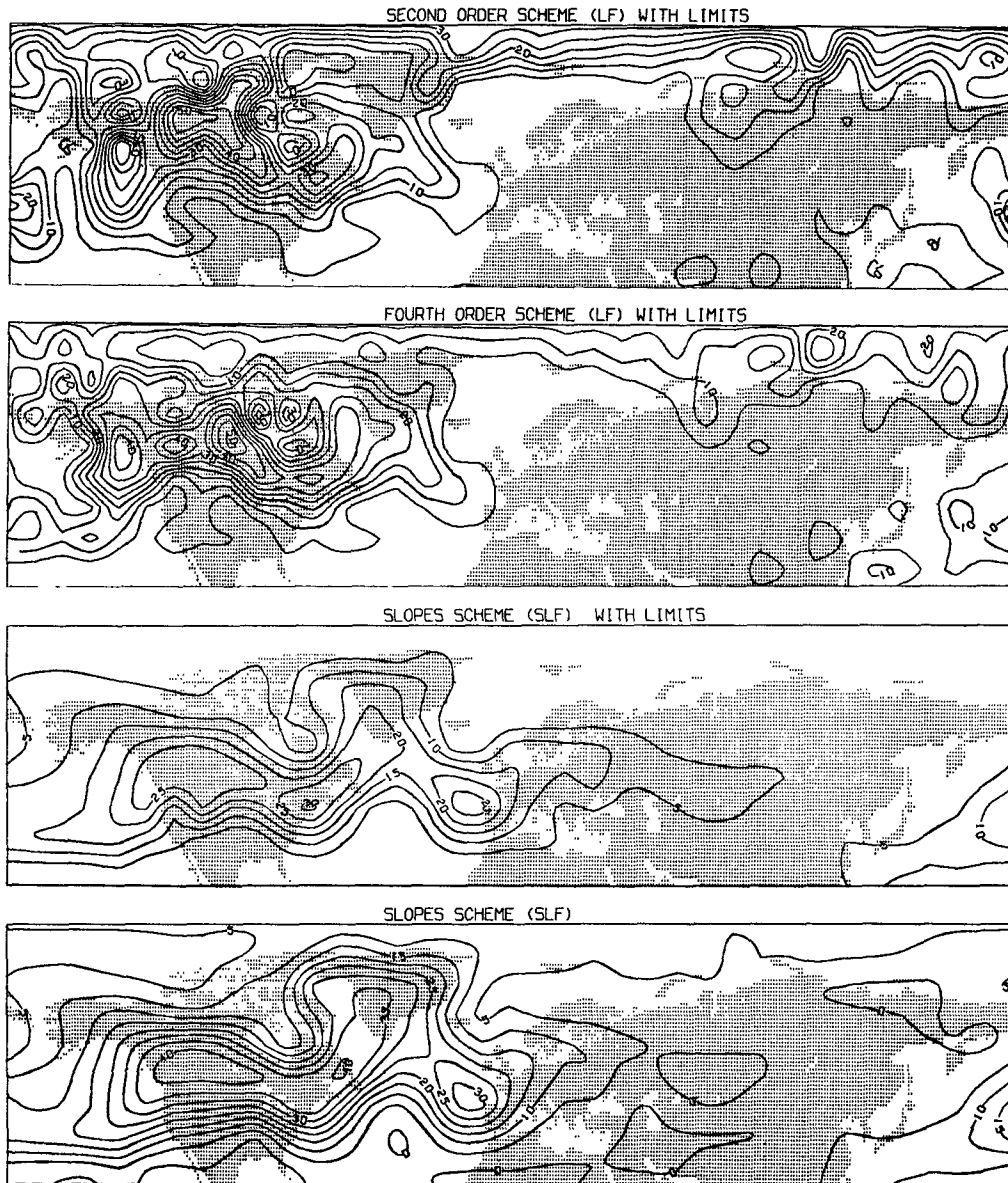SLOPES SCHEME (SLF) WITH LIMITS

SLOPES SCHEME (SLF)

FIG. 13. Fifth-layer concentrations for the schemes after 16 days of integration. The schemes
with limits and the slopes (SLF) scheme without limits are shown.

This condition persists when the experiments are extended and is caused by insufficient vertical mixing between the layers. Tropospheric convection can eliminate the negative concentrations in layers one and three, but the problem in the top layer is difficult to solve. Nevertheless, the slopes schemes are generally realistic and stable.

We also ran the experiments imposing "limits" that prevent negative concentrations. In the second- and fourth-order schemes, the tracer mass leaving a grid box during a time step is limited to the tracer mass in the box. In the slopes (SLF) scheme, each spatial gradient is limited in magnitude so that the concentration at the edge of a grid box is non-neg-

ative. As mentioned in the Introduction, such limits are not always useful.

Fig. 12 shows the fifth layer concentration predicted by the second- and fourth-order and the slopes (SLF) schemes with limits after four days. The schemes are in general agreement about the location of the ash cloud, although the second-order scheme still shows a slight lag and a single maximum.

When the experiments were extended an additional 12 days (Fig. 13), a tendency of the second- and fourth-order schemes to predict multiple minima and maxima with steep gradients became evident. Because their limits are frequently being imposed near the poles, the schemes have a tendency to ac-

TABLE 11. Relative computing time for the various schemes.

	Upstream	2nd order	4th order	Slopes	Slopes (SLF)
Pure form	0.81	1.00	1.54	3.00	1.93
With limits		1.99	2.31		2.62

cumulate concentration there. Despite their differences, all the schemes generally predict a maximum concentration over Canada with a wedge of low concentration butting into Hudson Bay.

Table 11 shows the relative computing time required for the various schemes in our three-dimensional model. For this table, the primary time step for all the schemes is 1 h including 1 h for the east-west advection of the slopes (SLF) scheme (and hence 2 h for the north-south advection and 4 h for vertical advection). The slopes schemes also require additional computer memory.

7. Conclusions

We have shown that the slopes method of solving the tracer transport equation is more accurate and reliable than the conventional formulations. In our periodic and three-dimensional models we saw that the pure second- and fourth-order schemes become totally unrealistic when the air mass is not uniform. We also have shown that both the upstream and slopes schemes are quite stable under these same conditions, but that the upstream scheme is much too diffuse.

Air mass variations occur in most applications, so it is important to understand why the various schemes behave so differently when perturbed in this way. In our three-dimensional model these air mass variations are caused primarily by the earth's irregular topography. Another contributing factor may be the rapid decrease in area (and mass) as the grid boxes approach the poles.

To explain the difficulties that occur with the second- and fourth-order schemes, one must first understand the mass reference frame. It is a Lagrangian reference frame in which a parcel of air always keeps the same mass coordinates. Since each parcel maintains the same tracer concentration for all time, concentration is a function only of the mass coordinates, independent of time. If an observer in a spatial reference frame could watch a tracer model run, he would see a fixed grid with air and tracer moving around him. If he were in a mass reference frame and watched the same experiment run, the tracer and air parcels would remain fixed, while the spatial grid lines would move around and become distorted. These ideas are illustrated in Fig. 2.

The second- and fourth-order schemes need to obtain the concentration at the grid box edges, which will multiply the air mass flux crossing an edge. To do this, the schemes interpolate assuming uniformly distributed grid boxes. That seems correct if things are viewed in the spatial reference frame. However, it is not correct when viewed through the mass reference frame. Tracer concentration is defined relative to air mass and not relative to space. In fact, with nonuniform mass, the second- and fourth-order schemes become first-order schemes in space.

By contrast, the upstream and slopes schemes view the concentration function as defined everywhere in the mass reference frame. At the end of each time step, when the numerical model's grid boxes are delineated, they refit the concentration by a constant or linear function for each box on the mass coordinates.

Versions of the second-order scheme with limits are widely used, yet we have seen in our model that the reliability of its predictions decreases after several simulated days. The fourth-order scheme, which seems more promising in the one-dimensional case, develops similar problems in our three-dimensional model. Our own experience with second- and fourth-order schemes in our three-dimensional tracer models is that at any time ~1% of the grid boxes have exceedingly low concentrations. In addition, tracer mass tends to accumulate at the poles.

The slopes scheme, while requiring considerably more programming effort, is more accurate and also is useful in applications with both positive and negative concentrations. Our full tracer model with the slopes (SLF) scheme uses subgrid-scale convection as determined by our general circulation model. The convection mixes vertically the mean concentration and the east-west and north-south slopes. The vertical slope is reduced proportional to the percentage of the grid box that is participating in the convection. The slopes scheme does not need nor use explicit diffusion.

In conclusion, we would add that the knowledge gained by studying the second- and fourth-order schemes in our tracer experiments can shed light on the behavior of these schemes when used in general circulation models.

REFERENCES

Anderson, D., and B. Fattahi, 1974: A comparison of numerical solutions of the advective equation. *J. Atmos. Sci.*, **31,** 1500–1506.

Crowley, W. P., 1968: Numerical advection experiments. *Mon. Wea. Rev.*, **96,** 1–11.

Hansen, J., G. Russell, D. Rind, P. Stone, A. Lacis, S. Lebedeff, R. Ruedy and L. Travis, 1982: Efficient three dimensional global models for climate studies. To be submitted to *J. Atmos. Sci.*

Kreiss, H., and J. Oliger, 1972: Comparison of accurate methods for the integration of hyperbolic equations. *Tellus*, **24,** 199–215.

Mahlman, J. D., and R. W. Sinclair, 1977: Tests of various numerical algorithms applied to a simple trace constituent air transport problem. *Fate of Pollutants in the Air and Water Environments*, I. H. Suffet, Ed., Wiley, 223–252.

Purnell, D. K., 1976, Solution of the advective equation by upstream interpolation with a cubic spline. *Mon. Wea. Rev.*, **104,** 42–48.